Nucleic Acid Delivery

International Edition: DOI: 10.1002/anie.201601273
German Edition: DOI: 10.1002/ange.201601273

Ultra-pH-Responsive and Tumor-Penetrating Nanoplatform for Targeted siRNA Delivery with Robust Anti-Cancer Efficacy

Xiaoding Xu+, Jun Wu+, Yanlan Liu, Mikyung Yu, Lili Zhao, Xi Zhu, Sushant Bhasin, Qing Li, Emily Ha, Jinjun Shi, and Omid C. Farokhzad**

Abstract: *RNA interference (RNAi) gene silencing technologies have shown significant potential for treating various diseases, including cancer. However, clinical success in cancer therapy remains elusive, mainly owing to suboptimal in vivo delivery of RNAi therapeutics such as small interference RNA (siRNA) to tumors. Herein, we developed a library of polymers that respond to a narrow pH change (ultra-pH-responsive), and demonstrated the utility of these materials in targeted and deep tumor-penetrating nanoparticle (NP) for in vivo RNAi. The new NP platform is mainly composed of the following key components: i) internalizing RGD (iRGD) to enhance tumor targeting and tissue penetration; ii) polyethylene glycol (PEG) chains to prolong blood circulation; and iii) sharp pH-responsive hydrophobic polymer to improve endosome escape. Through systematic studies of structure–function relationship, the optimized RNAi NPs (< 70 nm) showed efficient gene silencing and significant inhibition of tumor growth with negligible toxicities in vivo.*

RNAi technology has gained broad interest among academic and industry investigators for its potential to treat a myriad of diseases.[1a,b] One major hurdle in clinical translation of RNAi therapeutics (for example, siRNA) may be attributed to the lack of effective and non-toxic delivery vehicles to transport siRNA into diseased tissues and cells.[2] Specifically for cancer therapy, the barriers to effective in vivo siRNA delivery mainly include targeting to tumor, penetrating tumor tissue and cell membrane, escaping the endosome, and releasing siRNAs in the cytoplasm.[2] In the past decade, a variety of NP platforms made with cationic lipids,[3] polymers,[4] or lipid/polymer hybrids[5] have been demonstrated to significantly improve siRNA transfection in vitro. Nevertheless, their in vivo therapeutic efficacy is still limited by unsatisfactory blood circulation, poor tissue penetration, and endosomal entrapment.

[*] Dr. X. Xu,[+] Dr. J. Wu,[+] Dr. Y. Liu, Dr. M. Yu, Dr. L. Zhao, Dr. X. Zhu, S. Bhasin, Q. Li, E. Ha, Prof. J. Shi, Prof. O. C. Farokhzad
Department of Anesthesiology
Brigham and Women's Hospital
Harvard Medical School
Boston, MA 02115 (USA)
E-mail: jshi@bwh.harvard.edu
ofarokhzad@bwh.harvard.edu
Prof. O. C. Farokhzad
King Abdulaziz University
Jeddah (Saudi Arabia)
[+] These authors contributed equally to this work.

Supporting information for this article can be found under: http://dx.doi.org/10.1002/anie.201601273.

Aiming for effective in vivo delivery of siRNA to tumor cells, it is highly necessary to understand the obstacles from tumor tissues. The vasculature of solid tumors is fenestrate, through which NPs can extravasate and accumulate in tumors by the enhanced permeability and retention (EPR) effect.[6] However, efficiently crossing the vascular wall and penetrating deep into the tumor parenchyma against the elevated interstitial pressure remains an intractable problem.[7] In addition, the subsequent endosomal entrapment is another key bottleneck for the widespread use of siRNA therapeutics. Therefore, an ideal platform for safe and effective siRNA delivery to tumors should possess at least the following features: i) long blood circulation for high EPR effect and tumor accumulation; ii) capability for suitable tissue penetration and tumor-cell-targeting; iii) efficient endosomal escape for cytosolic delivery of the active siRNA; iv) biocompatibility of the material; and v) robust formulation processes that are amenable to scale-up using standard unit operations. To the best of our knowledge, a technology platform capable of satisfying all of these criteria has not been developed.

Herein, we developed a long-circulating, tumor-penetrating, and ultra-pH-responsive NP platform for effective in vivo siRNA delivery. This platform is made of a new PEGylated polymer, which shows an ultra-pH-responsive characteristic with a pK_a close to the endosomal pH (6.0–6.5),[8] and a tumor-penetrating peptide iRGD (Scheme 1 A,B). After encapsulating siRNA, the resulting delivery system shows four unique features (Scheme 1 C): i) the surface-encoded iRGD peptide endows the NPs with tumor-targeting and tumor-penetrating abilities; ii) the hydrophilic PEG shells prolong the blood circulation; iii) a small population of cationic lipid-like grafts randomly dispersed in the hydrophobic poly(2-(diisopropylamino) ethylmethacrylate) (PDPA) segment can entrap siRNA in the hydrophobic cores of the NPs; iv) the rapid protonation of the ultra-pH-responsive PDPA segment induces the endosomal swelling through the "proton sponge" effect, which synergizes with the insertion of the cationic lipid-like grafts into the endosomal membrane to induce membrane destabilization[9] and efficient endosomal escape.

The amphiphilic polymer, methoxyl-polyethylene glycol-*b*-poly (2-(diisopropylamino) ethylmethacrylate-*co*-glycidyl methacrylate) (Meo-PEG-*b*-P(DPA-*co*-GMA)), was first synthesized (Supporting Information, Scheme S1 and Table S1) and then further grafted by tetraethylenepentamine (TEPA) and 1,2-epoxyhexadecane to obtain Meo-PEG-*b*-P(DPA-*co*-GMA-TEPA-C14) (Scheme 1 A). We varied the length of the PDPA segment to adjust siRNA encapsulation

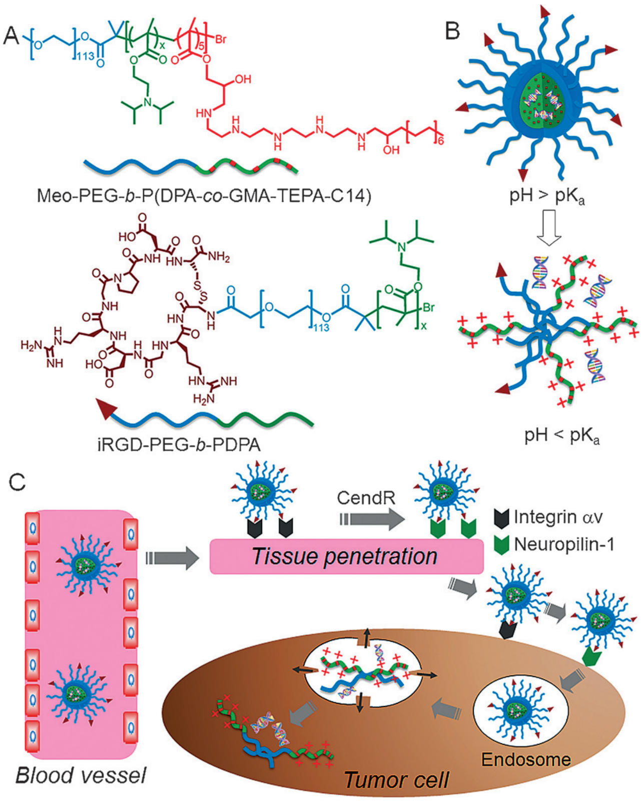

Scheme 1. A) Molecular structures of the ultra-pH-responsive polymer, Meo-PEG-*b*-P(DPA-*co*-GMA-TEPA-C14), and the tumor-penetrating polymer, iRGD-PEG-*b*-PDPA. B) Ultra-pH-responsive and tumor-penetrating nanoplatform for siRNA loading and release. C) Illustration of the nanoplatform for targeted in vivo siRNA delivery and cancer therapy. The iRGD-conjugated NPs target tumor tissue through the specific recognition between the RGD motif and αv-integrin-expressing endothelial cells in tumor tissue. Subsequently, the iRGD peptide is cleaved by cell-surface proteases to expose CRGDR sequence, which can bind to neuropilin-1 to induce penetration of tumor tissue and cells. After cellular uptake, the rapid protonation of the PDPA segment induces the endosomal swelling, which synergizes with the insertion of the cationic lipid-like grafts into the endosomal membrane to induce rapid endosomal escape and efficient gene silencing.

efficiency (EE%). As the PDPA length increased, the EE% and size of the resulting NPs increased (Table S3), possibly because the increased PDPA length led to an increase in the size of the hydrophobic core. Specifically, the EE% reached nearly 100% for the polymer with 80 ($PDPA_{80}$) or 100 ($PDPA_{100}$) DPA repeat units. Notably, using a mixture of Meo-PEG-*b*-P(DPA-*co*-GMA-TEPA-C14) (90 mol%) and tumor-penetrating polymer (iRGD-PEG-*b*-PDPA, 10 mol%; Scheme 1A) to prepare NPs did not cause obvious changes in the EE% or particle size (Table S4).

The polymer, $PDPA_{80}$ (pK_a 6.24, Table S3), was chosen for pH-response evaluation by incorporating a near-infrared dye, Cy5.5, into its PDPA segment (Scheme S2). Owing to the quenching of the aggregated fluorophores inside the hydrophobic cores of the NPs,[8] there was no fluorescence signal at a pH above the pK_a of $PDPA_{80}$ (Figure 1A). In contrast, at a pH below the pK_a, the protonated PDPA segment induced the disassembly of the NPs and a dramatic increase in the

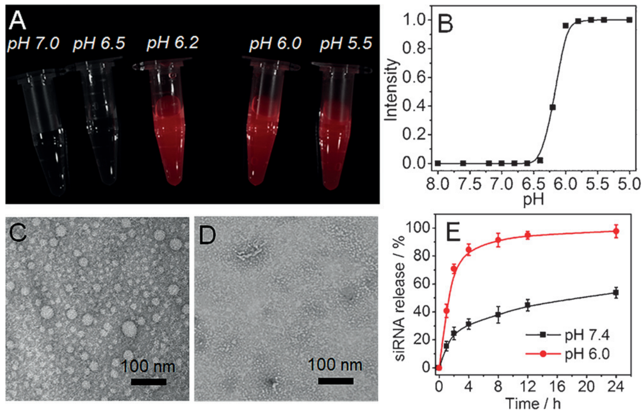

Figure 1. A) Fluorescent image of the Cy.5.5-labelled NPs of $PDPA_{80}$ at different pHs. B) Normalized fluorescence intensity as a function of pH for the Cy.5.5-labelled NPs of $PDPA_{80}$. TEM images of the siRNA-loaded NPs of $PDPA_{80}$ at a pH of C) 6.5 and D) 6.0. E) In vitro siRNA release from the NPs of $PDPA_{80}$ at 37°C.

fluorescence signal. Measurement of the fluorescence intensity upon pH change revealed that the pH difference from 10 to 90% fluorescence activation ($\Delta pH_{10-90\%}$) was 0.34 (Figure 1B and Table S3),[8] which is much smaller than that of small molecule dyes (about 2 pH units),[10] indicating the narrow pH response of $PDPA_{80}$. This characteristic was confirmed by transmission electron microscope (TEM). The spherical siRNA-loaded NPs could be visualized at a pH of 6.5 (Figure 1C), with an average size of 69.7 nm as determined by dynamic light scattering (DLS, Table S3). When the pH was altered to 6.0, there were no observable NPs after 20 min incubation (Figure 1D). With this morphological change, the NPs offered rapid release of DY547-labelled GL3 siRNA (DY547-siRNA; Figure 1E). Around 90% of the loaded siRNA was released within 4 h at a pH of 6.0. Within the same time frame, less than 30% of the loaded siRNA was released at a pH of 7.4.

Luciferase-expressing HeLa (Luc-HeLa) cells were used to evaluate the gene silencing efficacy. GL3 siRNA was employed to suppress luciferase expression. All of the siRNA-loaded NPs showed a reduction in luciferase expression at a 10 nM siRNA dose (Figure 2A), with the differential silencing efficacy depending upon the polymer structure. In comparison, the NPs with iRGD peptide (denoted iRGD-NPs) offered much better gene silencing efficacy. In particular, the iRGD-NPs_{80} prepared from $PDPA_{80}$ showed the best gene silencing efficacy, that is, >90% knockdown in luciferase expression without obvious cytotoxicity (Figure S4).

After acquiring the nanoplatform with optimal silencing efficacy (iRGD-NPs_{80}), flow cytometry was employed to evaluate its in vitro tumor-targeting ability. With the specific recognition between integrins ($\alpha_v\beta_3$ and $\alpha_v\beta_5$; Figure S5) on Luc-HeLa cells and iRGD, the uptake of DY547-siRNA-loaded iRGD-NPs_{80} was 3-fold higher than that of iRGD-absent NPs_{80} (Figures 2B and S6), demonstrating the excellent tumor-targeting ability of iRGD-NPs_{80}. The endosomal escape ability was assessed by staining the endosomes with LysoTracker Green. As shown in Figure 2C, a majority of the internalized siRNA-loaded NPs entered the cytoplasm after

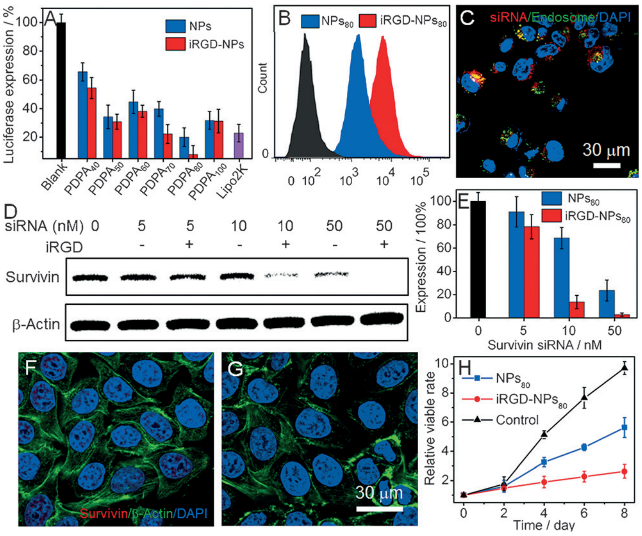

Figure 2. A) Luciferase expression in Luc-HeLa cells transfected with siRNA-loaded NPs at a 10 nm siRNA dose. B) Flow cytometry profile of Luc-HeLa cells incubated with the siRNA-loaded NPs_{80} and iRGD-NPs_{80} for 4 h. C) Fluorescent image of Luc-HeLa cells incubated with the siRNA-loaded iRGD-NPs_{80} for 4 h. D, E) Western blot analysis of survivin expression in PC3 cells treated by survivin siRNA-loaded NPs_{80} and iRGD-NPs_{80}. Fluorescent images of PC3 cells treated by anti-survivin siRNA-loaded F) NPs_{80} and G) iRGD-NPs_{80} at a 10 nm siRNA dose. H) Proliferation profile of PC3 cells incubated with anti-survivin siRNA-loaded NPs_{80} and iRGD-NPs_{80} at a 10 nm siRNA dose. Anti-GL3 siRNA-loaded NPs_{80} were used as a control.

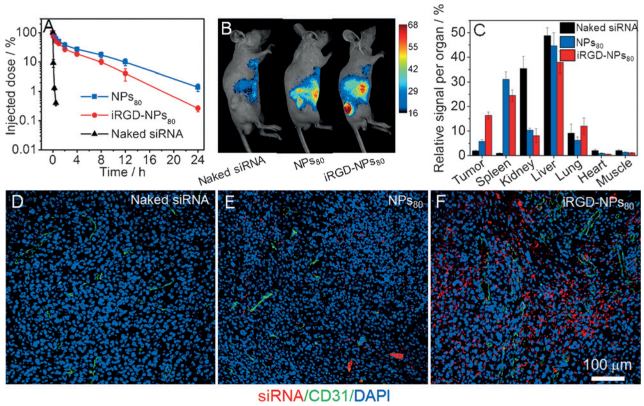

Figure 3. A) Pharmacokinetics of naked siRNA and siRNA-loaded NPs. B) Overlaid fluorescent image of PC3 xenograft-tumor-bearing mice at 24 h post-injection of naked siRNA and siRNA-loaded NPs. C) Biodistribution of the NPs in the PC3 xenograft-tumor-bearing mice sacrificed at 24 h post-injection of naked siRNA and siRNA-loaded NPs. Fluorescent images of the tumor sections of the PC3 xenograft-tumor-bearing mice sacrificed at 4 h post-injection of D) naked siRNA, E) siRNA-loaded NPs_{80}, and F) iRGD-NPs_{80}.

4 h incubation, indicating the effective endosomal escape of the iRGD-NPs_{80}. In comparison, for the iRGD-NPs prepared from polymer without lipid-like grafts or pH response (Scheme S4), the endosome escape ability was relatively weaker (Figure S8), thus leading to a much lower silencing efficacy (Figure S9).

We next examined whether the iRGD-NPs_{80} can be used to downregulate survivin expression, an inhibitor of apoptosis protein that is over-expressed in most cancers.[11] PC3 cells, a prostate cancer cell line showing targeted uptake of iRGD-NPs (Figures S5 and S6), were used as a model cell line. Western blot analysis (Figure 2D) indicated that the anti-survivin siRNA-loaded iRGD-NPs_{80} significantly suppressed survivin expression (> 80 % knockdown) at a 10 nm siRNA dose. At a 50 nm siRNA dose, survivin expression was nearly absent (< 3 %; Figure 2E). Similar results were also found in the immunofluorescence staining analysis (Figures 2F and 2G). Very weak red fluorescence corresponding to the residual survivin was observed in the cells treated with iRGD-NPs_{80} at a 10 nm siRNA dose (Figure 2G). With such suppressed survivin expression, the proliferation rate of PC3 cells was very slow. There was only 2.5-fold increase in cell number after 8 days incubation (Figure 2H).

After validating the efficient gene silencing, we then assessed the in vivo tumor-targeting ability of iRGD-NPs_{80}. The pharmacokinetics was first examined by intravenous injection of DY647-siRNA-loaded NPs. As shown in Figure 3A, the blood half-life ($t_{1/2}$) of iRGD-NPs_{80} was around 3.56 h, which is far longer than that of naked siRNA ($t_{1/2}$ < 30 min). This prolonged blood circulation was mainly due to the protection of PEG outer layer and small particle size.[12] The in vivo tumor-targeting ability was evaluated by intravenously injecting DY677-siRNA-loaded NPs into PC3 xenograft-tumor-bearing mice. As shown in Figure 3B, with the iRGD-mediated tumor-targeting, the iRGD-NPs_{80} showed a much higher tumor accumulation than that of NPs_{80} at 24 h post-injection. The tumors and main organs were harvested (Figure S11), and the NP biodistribution is shown in Figure 3C. Naked siRNA had a characteristic biodistribution, that is, high accumulation in the kidney but extremely low accumulation in the tumor. With the specific recognition between iRGD and integrins $\alpha_v\beta_3$ and $\alpha_v\beta_5$ over-expressed on tumor cells and angiogenic tumor vasculature,[8,13] the tumor accumulation of the iRGD-NPs_{80} was around 3-fold higher than that of NPs_{80}.

To evaluate the tumor-penetrating ability of the iRGD-NPs_{80}, the tumors were collected at 4 h post-injection of the DY677-siRNA-loaded NPs and then sectioned for immunofluorescence staining. As shown in Figure 3D, there was nearly no naked siRNA in the tumor section. For the NPs_{80} (Figure 3E), the number of NPs in the tumor section is very low. Additionally, most of these NPs were positioned in the tumor vessels, and only a small number reached the extravascular tumor parenchyma. In contrast, highly concentrated iRGD-NPs_{80} with bright red fluorescence could be visualized in the tumor section (Figure 3F). Remarkably, a majority of these NPs could cross tumor vessels and reach the extravascular tumor parenchyma, strongly demonstrating the deep tumor-penetrating characteristic of iRGD-NPs_{80}.

Finally, we evaluated the in vivo inhibition of survivin expression and anti-cancer efficacy. The anti-survivin siRNA-loaded NPs were intravenously injected into the PC3 xenograft-tumor-bearing mice (650 µg kg^{-1} siRNA dose, $n=3$) for three consecutive days. The siRNA-loaded NPs indeed suppressed survivin expression in the tumor (Figure 4A). In particular, the administration of iRGD-NP_{80} induced > 60 %

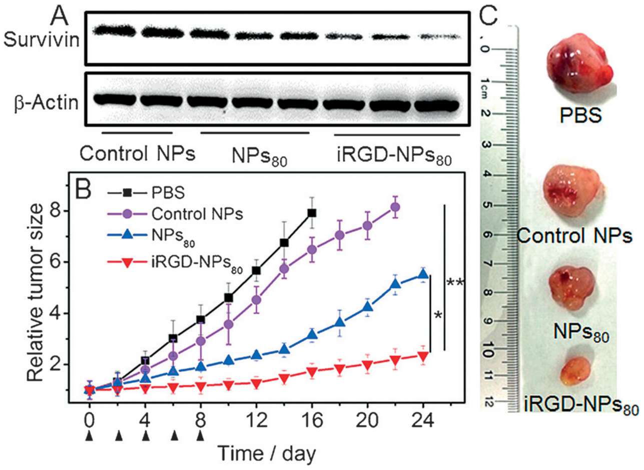

Figure 4. A) Western blot analysis of survivin expression in the PC3 tumor tissue after systemic treatment by control NPs and anti-survivin siRNA-loaded NPs. B) Relative tumor size of the PC3 xenograft-tumor-bearing mice after treatment by PBS, control NPs, and anti-survivin siRNA-loaded NPs. The intravenous injections are indicated by the arrows. C) Representative image of the harvested PC3 tumor from each group at day 16. Anti-GL3 siRNA-loaded NPs_{80} were used as a control. * $P<0.05$; ** $P<0.01$

knockdown in survivin expression (Figure S12), which was around 3-fold greater than that of NPs_{80}. Notably, the administration of NPs showed negligible in vivo side effects (Figure S13). To confirm that the NP-mediated survivin silencing had an anti-cancer effect, the anti-survivin siRNA-loaded NPs were intravenously injected into the mice once every two days at a 650 $\mu g\,kg^{-1}$ siRNA dose ($n=5$). After five consecutive injections (Figure 4B), the tumor growth was inhibited compared to the mice treated with PBS or anti-GL3 siRNA-loaded NPs (Control NPs). Particularly, with the excellent tumor-targeting and penetrating abilities, the iRGD-NPs_{80} could significantly suppress tumor growth, and there was only around a 2-fold increase in tumor size at day 24 (Figure 4C).

In summary, we successfully developed an ultra-pH-responsive and tumor-penetrating nanoplatform for targeted siRNA delivery. The in vitro and in vivo results demonstrated that this polymeric NP has a long blood circulation, and can efficiently target tumors and penetrate the tumor parenchyma, leading to efficient gene silencing and tumor growth inhibition. The polymeric nanoplatform reported herein may represent a robust siRNA delivery vehicle for the treatment of a myriad of important diseases, including cancer.

Acknowledgements

This work was supported by the NIH grants EB015419 (O.C.F), CA151884 (O.C.F.), R00CA160350 (J.S.), and CA200900 (J.S.); the Movember-Prostate Cancer Foundation (PCF) Challenge Award (O.C.F. and J.S.); the David H. Koch-PCF Program in Cancer Nanotherapeutics (O.C.F.); the PCF Young Investigator Award (J.S.); the Department of Defense Prostate Cancer Research Program Synergistic Idea Development Award (O.C.F. and J.S.); and the National Research Foundation of Korea grant K1A1A2048701 (O.C.F.). O.C.F. has financial interest in BIND Therapeutics, Selecta Biosciences, and Tarveda Therapeutics.

Keywords: cancer therapy · nanoparticles · pH-responsive · siRNA delivery · tumor penetration

How to cite: *Angew. Chem. Int. Ed.* **2016**, *55*, 7091–7094
Angew. Chem. **2016**, *128*, 7207–7210

[1] a) H. Yin, R. L. Kanasty, A. A. Eltoukhy, A. J. Vegas, J. R. Dorkin, D. G. Anderson, *Nat. Rev. Genet.* **2014**, *15*, 541–555; b) W. Sun, W. Ji, J. M. Hall, Q. Hu, C. Wang, C. L. Beisel, Z. Gu, *Angew. Chem. Int. Ed.* **2015**, *54*, 12029–12033; *Angew. Chem.* **2015**, *127*, 12197–12201.
[2] K. A. Whitehead, R. Langer, D. G. Anderson, *Nat. Rev. Drug Discovery* **2009**, *8*, 129–138.
[3] Y.-C. Tseng, S. Mozumdar, L. Huang, *Adv. Drug Delivery Rev.* **2009**, *61*, 721–731.
[4] Y. Zhang, A. Satterlee, L. Huang, *Mol. Ther.* **2012**, *20*, 1298–1304.
[5] J. Shi, Z. Xiao, A. R. Votruba, C. Vilos, O. C. Farokhzad, *Angew. Chem. Int. Ed.* **2011**, *50*, 7027–7031; *Angew. Chem.* **2011**, *123*, 7165–7169.
[6] O. C. Farokhzad, R. Langer, *ACS Nano* **2009**, *3*, 16–20.
[7] C.-H. Heldin, K. Rubin, K. Pietras, A. Ostman, *Nat. Rev. Cancer* **2004**, *4*, 806–813.
[8] Y. Wang, K. Zhou, G. Huang, C. Hensley, X. Huang, X. Ma, T. Zhao, B. D. Sumer, R. J. DeBerardinis, J. Gao, *Nat. Mater.* **2014**, *13*, 204–212.
[9] X. Zhu, Y. Xu, L. M. Solis, W. Tao, L. Wang, C. Behrens, X. Xu, L. Zhao, D. Liu, J. Wu, N. Zhang, I. I. Wistuba, O. C. Farokhzad, B. R. Zetter, J. Shi, *Proc. Natl. Acad. Sci. USA* **2015**, *112*, 7779–7784.
[10] Y. Urano, D. Asanuma, Y. Hama, Y. Koyama, T. Barrett, M. Kamiya, T. Nagano, T. Watanabe, A. Hasegawa, P. L. Choyke, H. Kobayashi, *Nat. Med.* **2009**, *15*, 104–109.
[11] D. C. Altieri, *Nat. Rev. Cancer* **2003**, *3*, 46–54.
[12] K. Knop, R. Hoogenboom, D. Fischer, U. S. Schubert, *Angew. Chem. Int. Ed.* **2010**, *49*, 6288–6308; *Angew. Chem.* **2010**, *122*, 6430–6452.
[13] K. N. Sugahara, T. Teesalu, P. P. Karmali, V. R. Kotamraju, L. Agemy, O. M. Girard, D. Hanahan, R. F. Mattrey, E. Ruoslahti, *Cancer Cell* **2009**, *16*, 510–520.

Received: February 3, 2016
Published online: May 3, 2016